Electronic Supplementary Material (ESI) for Materials Advances.

Supporting Information

Environment Pollutant to Efficient Solar Vapor Generator; an Eco-Friendly Way of Freshwater Production

Tawseef A. Wani, Parul Garg, Ashok Bera*

Department of Physics, Indian Institute of Technology Jammu, Jammu and Kashmir, 181221 India

EXPERIMENTAL METHODS

Materials: Raw coconut husk was collected from coconut. KOH solution was prepared by dissolving 3 wt% KOH in de-ionized water.

Fabrication of CCH evaporator: To prepare CCH evaporators, raw coconut husk was cut into pieces, washed thoroughly using KOH solution followed by DI water. Then the husk was compressed tightly by a rope into a cylindrical shape followed by drying overnight at 70 °C in an oven. Finally, the dried cylindrical coconut husk was unroped (cylindrical shape was well maintained) and carbonized its cylindrical surfaces as well as top surface using a household LPG stove in an environmental condition. To restrict the carbonization only to the surface of CCH, the flaming process was limited to a short period followed by dipping in DI water for the 60s that prevent the internal part from burning.

Material characterizations: Cleaned coconut husk was cut into pieces followed by grinding to get virgin coconut husk for characterization. Carbonized coconut husk was collected by scratching the carbonized surfaces of the CCH evaporators. The structure and the morphology of the carbonized and virgin coconut husk were characterized by and Field emission scanning electron microscopy (Jeol JSM 7900F). The porosity and the samples' surface area were measured Brunauer–Emmett–Teller (Autosorb -IQ-XR-XR-AG) adsorption method. Chemical compositions of the sample were estimated by X-ray Photo-electron spectroscopy (Nexsa-ThermoFisher), and Fourier transformed infrared spectroscopy (Nicolet IS50 - Thermo scientific). The optical reflectance of the CCH was directly measured by a UV-Vis-NIR spectrophotometer (Agilent-Cary series) attached with an integrated sphere.

Vapor Generation measurement: The CCH steam generator was put on Polystyrene foam with a small hole in it through which water was supplied to the evaporator by using a cotton thread. Between the evaporator and the foam, an air-laid paper with the same area as that of the evaporator's bottom was placed to ensure a homogeneous water supply. Before starting the experiment, the SVG was placed on the container with thread soaking in water and kept overnight for complete water filling of the coconut husk's pores till the top of the evaporator. The evaporator was placed under a Xenon light source (66921, Newport Corporation) which was turned on when the water reached its top. Once the light falls on the evaporator, the mass change profile was measured by an analytical balance (ME204, Mettler Toledo). The intensity of light was adjusted at 1 Sun (1000 w m^{-2}) by calibrating with a thermopile sensor (919P-003-10, Newport Corporation) connected to a light meter (843-R, Newport Corporation). Due to the non-uniform distribution of light, the solar flux of different locations over the desired area was averaged to reduce the error. The infrared camera (FLIR E75) connected with a computer was used to record the temperature profile of the system. The area was measured at the maximum circumference of the cylindrical evaporator. All the experiments were conducted at an ambient temperature of ≈23 °C and relative humidity of ≈48%.

Note S1. Calculation of solar absorptance

Solar absorptance (α) is defined as a weighted fraction between absorbed radiation energy and incoming solar radiation energy and is given by the following equation [S1]

$$\alpha = \frac{\int_{\lambda_{min}}^{\lambda_{max}} (1 - R(\lambda))I(\lambda)d\lambda}{\int_{\lambda_{min}}^{\lambda_{max}} I(\lambda)d\lambda},$$

where λ is the wavelength, λ_{min} the minimum wavelength, λ_{max} the maximum wavelength, $I(\lambda)$ the light intensity function of the solar spectrum and $R(\lambda)$ the reflectivity function of the sample at different wavelength. λ_{min} and λ_{max} in our case were respectively 300 nm and 2500 nm.

Note S2. Calculation of energy efficiency

By using the total input energy and total energy loss, the energy efficiency can be calculated using Eq. (A.1) [S2-S4]

$$\eta = \frac{Q_{solar} + Q_{gain} - Q_{loss}}{Q_{solar} + Q_{gain}} \qquad (A.1)$$

where Q_{solar} input energy from the simulated solar light, Q_{gain} is the energy input from the surrounding environment, and Q_{loss} is the energy loss to the environment.

$$Q_{solar} = S_{top}q_{solar} \qquad (A.2)$$

$$Q_{gain} = S_{cur}\epsilon\sigma\left(T_{amb}^{4} - T_1^4\right) + S_{cur}h(T_{amb} - T_1) \qquad (A.3)$$

$$Q_{loss} = S_{top}Rq_{solar} + S_{top}\epsilon\sigma\left(T_2^4 - T_{amb}^{\ 4}\right) + S_{top}h(T_2 - T_{amb}) \qquad \text{(A.4)}$$

Where S_{top} is the projection area of the evaporator, q_{solar} is the solar flux (1000 W m^{-2}), S_{cur} is the curved surface area of the evaporator, ϵ is the emittance of the surface, σ is the Stefan-Boltzmann constant, T_{amb} is the temperature of the environment, T_1 is the temperature of the top surface of the evaporator, h is the heat transfer coefficient (10 W m^{-2} K^{-1}), R is the reflectivity of the evaporator, and T_2 is the temperature of the curved surface of the evaporator.

The illuminated area is 3.14 cm^2, so the total input energy from 1 sun (1000 kW m^{-2}) is 0 .314W. The three terms in Eq. (A.4) correspond to the reflective, radiative, and convective heat losses. The reflective loss is calculated as 0.0075 W (2.4% of 0.3141 W). The radiative energy and convective loss using T_2 = 31 °C, and T_{amb} = 23 °C were calculated as 0.0149 and 0.0266 W. Also, the radiative and convective energy gain (given by Eq. (A.3)) by the evaporator's curved surface from the environment are respectively 0.0426 and 0.1507 W. Therefore, the total energy loss and total energy gain are respectively 0.0490 and 0.1933 W.

The energy efficiency by taking only solar flux as the input energy is 145.9% ({0.314 + 0.1933 - 0.0490} / 0.314). The energy efficiency using total energy (0.314 + 0.1933) in the denominator gives the efficiency as 90.3%.

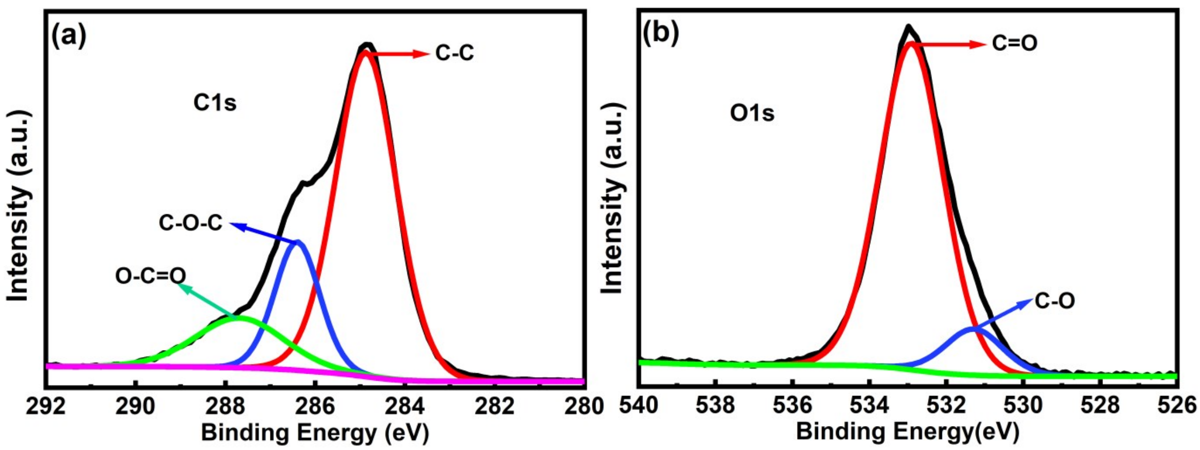

Fig. S1. High-resolution XPS spectra of (a) C1s and (b) O1s orbitals of coconut husk before carbonization

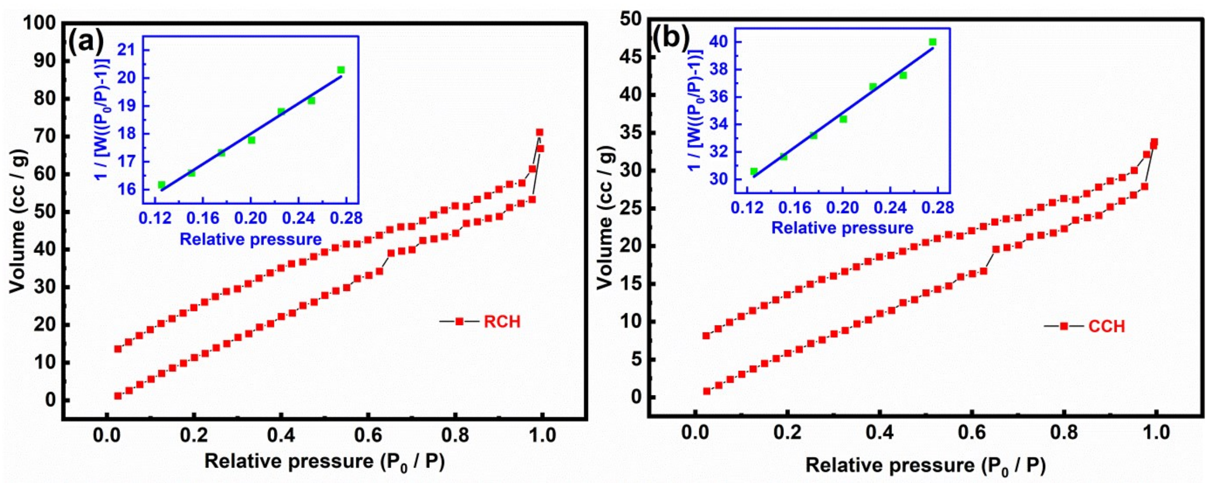

Fig. S2. N2-adsorption/desorption isotherms of (a) raw and (b) carbonized coconut husk. The insets show their respective multipoint BET curves.

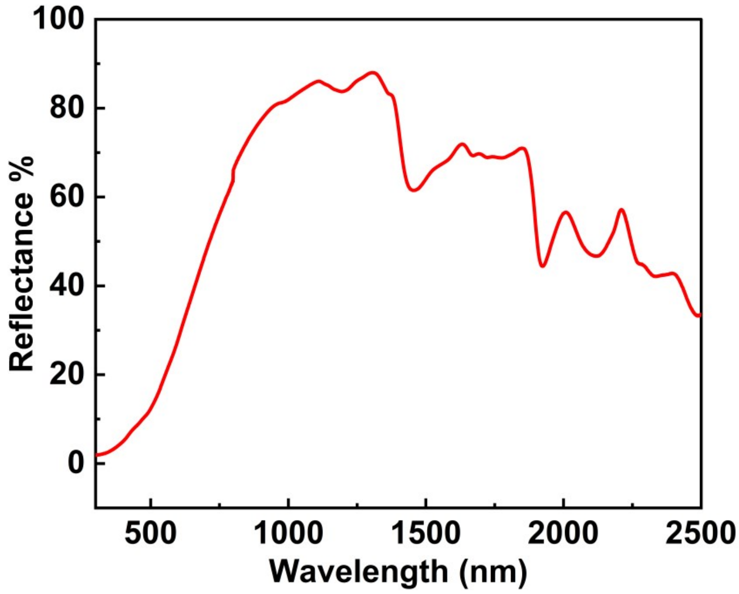

Fig. S3. UV-Vis-NIR spectum of raw coconut husk.

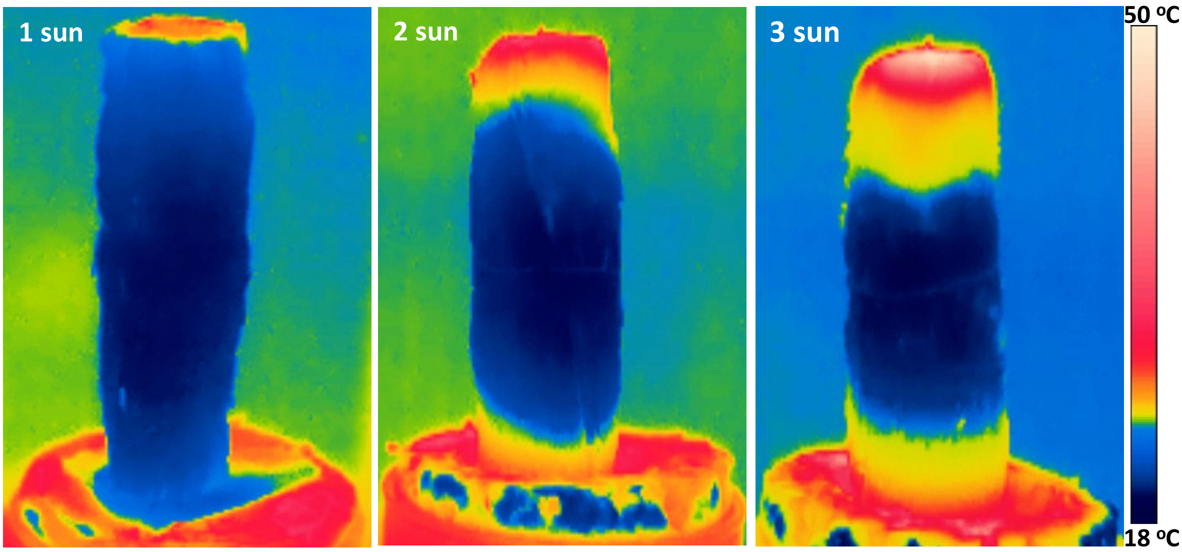

Fig. S4. IR thermal images of CCH evaporator at 1, 2, 3 sun after 1 h of illumination. These thermal images show the middle temperature is low, which confirms its high thermal conductivity and energy harvesting. The temperature increase at the lower side is due to the heating of polystyrene foam below the evaporator.

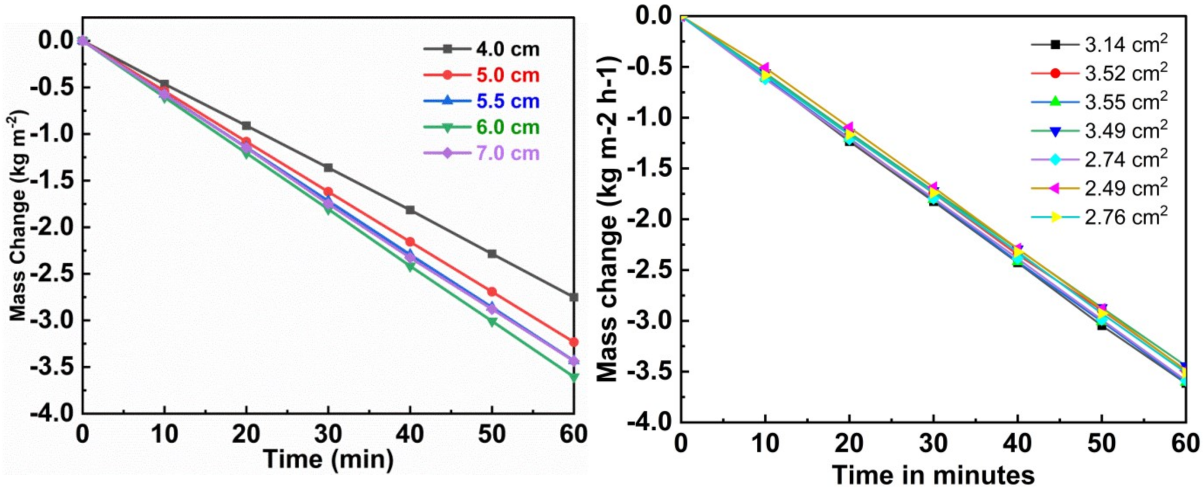

Fig. S5. (a) Mass change of CCH evaporator with different heights for 1 h after saturation, confirming the highest evaporation around the 6 cm height. (b) Mass change of CCH evaporator with silghlt varying areas with same height of 6 cm for 1 h after saturation

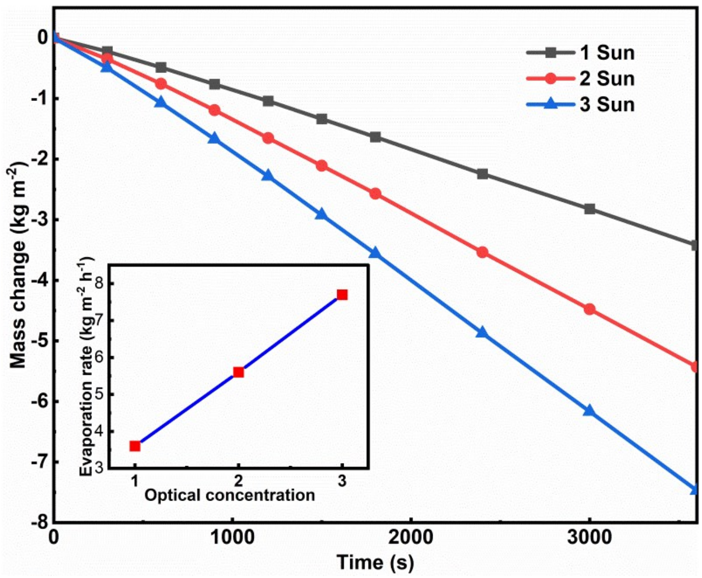

Fig. S6. Mass change of CCH evaporator at higher intensities. Inset shows the linearity of the evaporation rate with optical concentration**.**

Fig. S7. Photograph for the side view (left) and top view (right) of the prototype of CCH based solar steam generation.

Table S1. Comparison of evaporation rates of CCH evaporator with recently reported 3D evaporators.

Materials/evaporator	Structure	Solar intensity ($kW\ m^{-2}$)	Evaporation rate ($kg\ m^{-2}\ h^{-1}$)	Reference
Carbonized coconut husk	**3D**	**1.0**	**3.6**	**This work**
Cup structure using semiconductor nanoparticles	3D	1.0	2.04	S1
Tree-shaped PPy coated paper (leaf-shaped)	3D	1.0	2.3	S2

Polypyrrole-coated Setaria viridis spike composites	3D	1.0	3.72	S3
Nickle-cobalt@ polydopamine sponges	3D	1.0	2.42	S5
Vertically aligned activated carbon juncus effusus	3D	1.0	2.23	S6
Activated carbon-cotton fabric	3D	1.0	1.95	S7
Nanodiamonds paint filter paper	3D	1.0	1.32	S8
Ten-stage thermally-localized multistage solar still prototype	3D	1.0	5.78	S9
Polypyrole decorated maize straws	3D	1.0	3.0	S10
RGO-bamboo paper	3D	1.0	2.94	S11
Carbonized carrot	3D	1.0	2.04	S12
Carbon dot @cellulose paper	3D	1.0	2.93	S13
Ag-polydopamine core-shell structured NPs decorated on Wooden Flower	3D	1.0	2.08	S14

RGO-agrose-cotton aerogel	3D	1.0	4.0	S15
Black nylon fibers @ planar polyvinyl chloride	3D	1.0	2.09	S16
Carbonized sunflower heads	3D	1.0	1.51	S17
Carbonized bamboo	3D	1.0	3.13	S18
3D printed cone based on carbon nanotube	3D	1.0	2.63	S19
3D spiral structure	3D	1.0	4.35	S20
Carbonized mushroom	3D	1.0	1.48	S21

Table S2. Conductivity and pH values of different contaminated solutions before and after purification compared with that of DI and RO water.

S.No.	**Type of solution**	**Conductivity (mS/cm)**		**pH value**	
		Before	**After**	**Before**	**After**
1	Saltwater	197.20	0.079	8.881	7.563
2	Methylene blue	21.30	0.0071	1.575	7.399
3	Soap solution	1.80	0.107	12.00	7.749
4	Detergent solution	69.00	0.2110	10.405	7.903
5	DI water	0.00155		7.23	
6	RO water	0.132		7.69	

REFERENCES

(S1) Y. Shi, R. Li, Y. Jin, S. Zhuo, L. Shi, J. Chang, S. Hong, K. C. Ng and P. Wang, *Joule*, 2018, **2**, 1171–1186.

(S2) H. Wang, C. Zhang, Z. Zhang, B. Zhou, J. Shen and A. Du, *Adv. Funct. Mater.*, 2020, **30**, 1–10.

(S3) Z. Xie, J. Zhu and L. Zhang, *ACS Appl. Mater. Interfaces* 2021, **13**, 9027–9035.

(S4) G. Ni, G. Li, S. V. Boriskina, H. Li, W. Yang, T. J. Zhang and G. Chen, *Nat. Energy*, 2016, **1**, 1–7

(S5) B. Shao, Y. Wang, X. Wu, Y. Lu, X. Yang, G. Y. Chen, G. Owens and H. Xu, *J. Mater. Chem. A*, 2020, **8**, 11665–11673.

(S6) Q. Zhang, L. Ren, X. Xiao, Y. Chen, L. Xia, G. Zhao, H. Yang, X. Wang and W. Xu, *Carbon N. Y.*, 2020, **156**, 225–233.

(S7) Q. Zhang, R. Hu, Y. Chen, X. Xiao, G. Zhao, H. Yang, J. Li, W. Xu and X. Wang, *Appl. Energy*, 2020, **276**, 115545.

(S8) L. Zhang, B. Bai, N. Hu and H. Wang, *Appl. Therm. Eng.*, 2020, **171**, 115059.

(S9) Z. Xu, L. Zhang, L. Zhao, B. Li, B. Bhatia, C. Wang, K. L. Wilke, Y. Song, O. Labban, J. H. Lienhard, R. Wang and E. N. Wang, *Energy Environ. Sci.*, 2020, **13**, 830–839.

(S10) Y. Xu, C. Tang, J. Ma, D. Liu, D. Qi, S. You, F. Cui, Y. Wei and W. Wang, *Environ. Sci. Technol.*, 2020, **54**, 5150–5158.

(S11) Y. Wang, X. Wu, B. Shao, X. Yang, G. Owens and H. Xu, *Sci. Bull.*, 2020, **65**, 1380–

1388.

(S12) Y. Long, S. Huang, H. Yi, J. Chen, J. Wu, Q. Liao, H. Liang, H. Cui, S. Ruan and Y. J. Zeng, *J. Mater. Chem. A*, 2019, **7**, 26911–26916.

(S13) Z. Wang, W. Tu, Y. Zhao, H. Wang, H. Huang, Y. Liu, M. Shao, B. Yao and Z. Kang, *J. Mater. Chem. A*, 2020, **8**, 14566–14573.

(S14) S. Chen, Z. Sun, W. Xiang, C. Shen, Z. Wang, X. Jia, J. Sun and C. J. Liu, *Nano Energy*, 2020, **76**, 104998.

(S15) X. Wu, T. Gao, C. Han, J. Xu, G. Owens and H. Xu, *Sci. Bull.*, 2019, **64**, 1625–1633.

(S16) C. Tu, W. Cai, X. Chen, X. Ouyang, H. Zhang and Z. Zhang, *Small*, 2019, **15**, 1–8.

(S17) P. Sun, W. Zhang, I. Zada, Y. Zhang, J. Gu, Q. Liu, H. Su, D. Pantelić, B. Jelenković and D. Zhang, *ACS Appl. Mater. Interfaces*, 2020, **12**, 2171–2179.

(S18) Y. Bian, Q. Du, K. Tang, Y. Shen, L. Hao, D. Zhou, X. Wang, Z. Xu, H. Zhang, L. Zhao, S. Zhu, J. Ye and H. Lu, Adv. Mater. Technol. 2019, **4**, 1800593

(S19) L. Wu, Z. Dong, Z. Cai, T. Ganapathy, N. X. Fang, C. Li, C. Yu, Y. Zhang and Y. Song, *Nat. Commun.*, 2020, 11, 521.

(S20) Y. Wang, X. Wu, T. Gao, Y. Lu, X. Yang, G. Y. Chen, G. Owens and H. Xu, *Nano Energy*, 2020, **79**, 105477.

(S21) N. Xu, X. Hu, W. Xu, X. Li, L. Zhou, S. Zhu and J. Zhu, Adv. Mater. 2017, **29**, 1606762